


 Cite this: *RSC Adv.*, 2022, 12, 23937

# The adsorption behaviors of N<sub>2</sub>O on penta-graphene and Ni-doped penta-graphene

 Hu Hua<sup>ab</sup> and Yun Ni  <sup>\*ab</sup>

In order to develop the adsorption application of penta-graphene (PG) to N<sub>2</sub>O gas molecule, we calculated the sensing properties of PG and Ni-doped PG to N<sub>2</sub>O molecule *via* first-principles calculations. Based on the calculated adsorption energy, charge transfer, band gap, density of states and partial density of states, we observed that this gas molecule was weakly physically adsorbed on the surface of intrinsic PG, while the adsorption behaviors on the surface of Ni-doped PG were greatly influenced by the doping sites and adsorption orientations. With the Ni atom doped at the sp<sup>2</sup> hybridized carbon site, strong chemical adsorption between the gas molecule and the substrate was induced. The adsorption structure of the N<sub>2</sub>O molecule with its N atom close to the substrate exhibited better stability. Moreover, an external perpendicular electric field could enhance the adsorption performance of the N<sub>2</sub>O molecule and adjust the charge transfer between the molecule and substrate. Our results broaden the adsorption applications of PG and indicate that Ni-doped PG is a potential candidate for N<sub>2</sub>O gas sensors.

 Received 2nd June 2022  
 Accepted 9th August 2022

DOI: 10.1039/d2ra03424g

[rsc.li/rsc-advances](http://rsc.li/rsc-advances)

## 1. Introduction

Penta-graphene (PG) is a new two-dimensional material with a metastable carbon pentagonal structure. Compared with conventional hexagonal graphene, which has robust sp<sup>2</sup> binding among carbon atoms, PG contains both sp<sup>2</sup> and sp<sup>3</sup> hybridized carbon atoms.<sup>1</sup> The unique hybridized bonds enable PG exceptional mechanical properties,<sup>2</sup> low thermal conductivity,<sup>3</sup> compelling optical property,<sup>4</sup> ultrahigh carrier migration rate,<sup>5</sup> and energetic and dynamic stabilities.<sup>1</sup> Because of its excellent features, PG is anticipated to develop into a potential anode candidate for Li/Na-ion batteries,<sup>6</sup> a competitive and metal-free catalyst for CO oxidation at a low temperature,<sup>7</sup> and a potential gas sensor for some harmful gases.<sup>8–10</sup> The band gap of PG makes it a semiconductor, and the tetrahedral character of the sp<sup>3</sup>-hybridized carbon gives PG a buckle shape, which is not ideally planar but rather oscillates out-of-plane in a periodically corrugated manner. Therefore, PG can adsorb gas molecules in rich configurations, and it is considered a potential candidate for developing gas sensors.

Recently, the identification and elimination of harmful gases from carbon-based structures have attracted considerable attention. Many researchers have shifted their main focus from traditional 2D materials, such as graphene,<sup>11</sup> MoS<sub>2</sub> (ref. 12) and BN,<sup>13</sup> to other graphene-like 2D materials<sup>14–16</sup> and carbon-based materials, such as graphyne<sup>17</sup> and PG. It has

been reported that the CO, H<sub>2</sub>O, H<sub>2</sub>S, NH<sub>3</sub> and SO<sub>2</sub> gas molecules are physically adsorbed on intrinsic PG,<sup>18</sup> whereas the NO and NO<sub>2</sub> molecules on PG belong to chemisorption. Moreover, doping can improve the adsorption ability of gas molecules. It has also been reported that transition-metal-doped PG is a potential hydrogen-storage material<sup>19</sup> and Zhang<sup>20</sup> *et al.* observed that transition-metal-doped PG can significantly enhance the adsorption performance of CO and CO<sub>2</sub> gas molecules. However, to the best of our knowledge, no previous reports have focused on the adsorption behaviors of N<sub>2</sub>O gas molecules on the intrinsic and doped PG, which is highly desirable to be explored. N<sub>2</sub>O gas molecules mainly arise from the selective catalytic reduction of NO<sub>x</sub> and the burning of fossil fuels and biomass.<sup>21,22</sup> Since the excessive emission of N<sub>2</sub>O accelerates the exhaustion of ozone in the stratosphere,<sup>23</sup> it is necessary to lower the concentration level of N<sub>2</sub>O gas in chemical processes using highly sensitive materials with efficient adsorption performance.

Among the transition metal atoms, we mainly focus on the last three successive groups because they have filled and near filled d shell electrons. Moreover, for the sake of electrochemical stability and economic cost, we chose a cheap and promising metal, namely nickel, as the dopant in our study, which improved the admirable catalytic behavior<sup>24</sup> and outstanding gas adsorption application<sup>25,26</sup> in previous studies. Although the Ni-doped penta-graphene has not been synthesized experimentally, the Ni-doped graphene and intrinsic penta-graphene have been synthesized experimentally.<sup>27,28</sup> We believe that the synthesis of transition metal doped penta-graphene can be achieved in the near future. In our study, the sensing properties of PG and Ni-doped PG to the small gas

<sup>a</sup>Hubei Engineering Technology Research Center of Energy Photoelectric Device and System, Hubei University of Technology, Wuhan, 430068, China. E-mail: niyun@hbut.edu.cn

<sup>b</sup>College of Science, Hubei University of Technology, Wuhan, 430068, China



molecule  $\text{N}_2\text{O}$  were investigated *via* first-principles calculations. Based on the unique structure of PG, different doping sites and adsorption orientations were considered before adsorption. The adsorption energy, charge transfer, band gap, density of states, and partial density of states were calculated to analyze the different adsorption behaviors. Moreover, in order to enhance the adsorption performance of  $\text{N}_2\text{O}$  on the substrate, an external perpendicular electric field was employed to tune its adsorbability.

## 2. Methods

The projected-augmented wave (PAW) and plane wave basis method of the Vienna *ab initio* simulation package (VASP)<sup>29,30</sup> were utilized to calculate the adsorption of  $\text{N}_2\text{O}$  molecule *via* density functional theory (DFT).<sup>31</sup> For the exchange-correlation potential, the generalized gradient approximation (GGA)<sup>32</sup> of the Perdew–Burke–Ernzerhof (PBE)<sup>33</sup> function was applied. Since PBE function fails to precisely convey van der Waals interactions caused by the undulating movement of electric charge, the DFT-D2 method was used to solve this problem.<sup>34</sup> Spin polarization must be considered in the structural relaxation process. We constructed a  $3 \times 3 \times 1$  supercell PG containing 54 atoms. In the structural optimization process, the truncated energy was set to 520 eV, the  $k$ -point grid centered on gamma in the Brillouin zone was set to  $3 \times 3 \times 1$ , and the convergence condition was set to 0.1 meV. In order to obtain an accurate density of states, the mesh point of  $k$  space was increased to  $9 \times 9 \times 1$ . To eliminate the influence of the interaction between the adjoining PG layers, the height of the vacuum layer was set to 15 Å. The adsorption energy  $E_{\text{ad}}$  was calculated using the following formula:

$$E_{\text{ad}} = E_{\text{gas/substrate}} - E_{\text{gas}} - E_{\text{substrate}}, \quad (1)$$

where  $E_{\text{gas/substrate}}$ ,  $E_{\text{gas}}$  and  $E_{\text{substrate}}$  represent the total energies of  $\text{N}_2\text{O}$  adsorbed on the substrate, isolated  $\text{N}_2\text{O}$  molecule, and isolated substrate, respectively.

**Table 1** Calculated lattice constant, bond length and bond angle between adjacent C1 and C2 atoms of the optimized  $3 \times 3 \times 1$  PG sheet

Lattice constant (Å)	Bond length (Å)	Bond angle
$a = b = 10.920$	C1–C2 = 1.550	C2–C1–C2 = 134.386°
$c = 15.00$	C2–C2 = 1.339	C1–C2–C1 = 112.446°
		C2–C2–C1 = 113.498°

## 3. Results and discussion

### 3.1. The intrinsic PG

The optimized structure of the  $3 \times 3 \times 1$  supercell PG model is shown in Fig. 1a. The  $\text{sp}^3$  and  $\text{sp}^2$  hybridized carbon atoms are marked C1 and C2 in yellow and gray colors, respectively. The detailed parameters related to the PG sheet are shown in Table 1, which are consistent with previous studies.<sup>35</sup> The plane composed of C1 atoms was 0.604 Å away from the coplanar structure consisting of C2 atoms. The band structure and projected density of states (DOS) are shown in Fig. 1b. The intrinsic PG exhibits a band gap  $E_g = 2.21$  eV, and the primary contribution to the total DOS is derived from C2 atoms.

According to the structure of  $\text{N}_2\text{O}$  gas molecules, three orientations were considered before the adsorption calculation:  $\text{N}_2\text{O}$  molecule is vertical to the substrate end with O atom (O end),  $\text{N}_2\text{O}$  molecule is vertical to the substrate end with N atom (N end), and  $\text{N}_2\text{O}$  molecule is horizontal to the substrate. Because PG has two adsorption sites, C1 and C2,  $\text{N}_2\text{O}$  has six adsorption orientations, as shown in Fig. 2. The corresponding characteristic parameters (including adsorption distance, adsorption energy, band gap and charge transfer) are listed in Table 2. The results show that  $\text{N}_2\text{O}$  gas molecules with different adsorption orientations are far away from the PG sheet with adsorption distances from 2.638 Å to 2.994 Å, and the adsorption energies are quite small, ranging from  $-0.203$  eV to

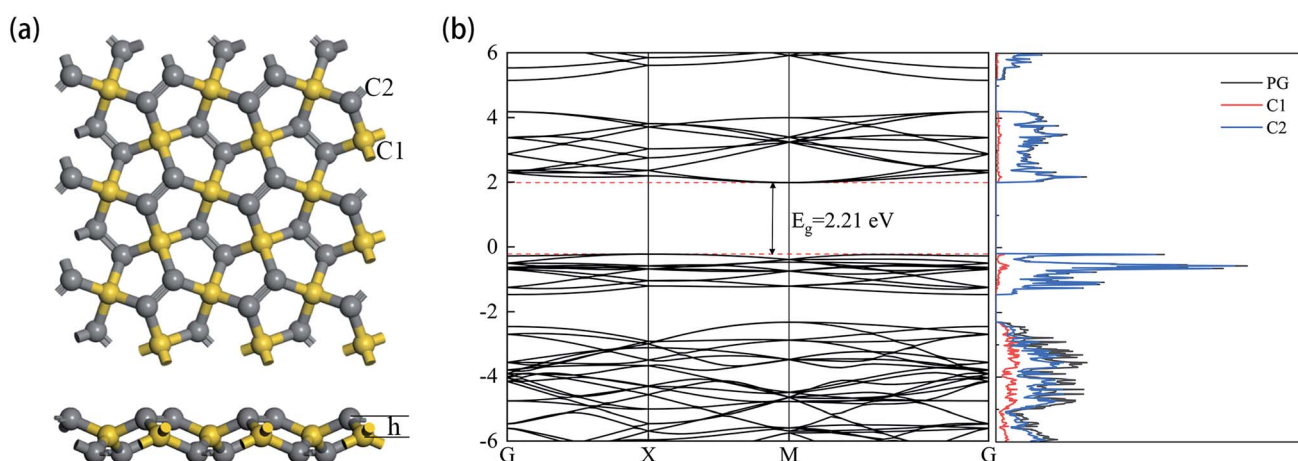


**Fig. 1** (a) Top and side views (b) the electronic band structure and density of the states of the relaxed PG sheet.



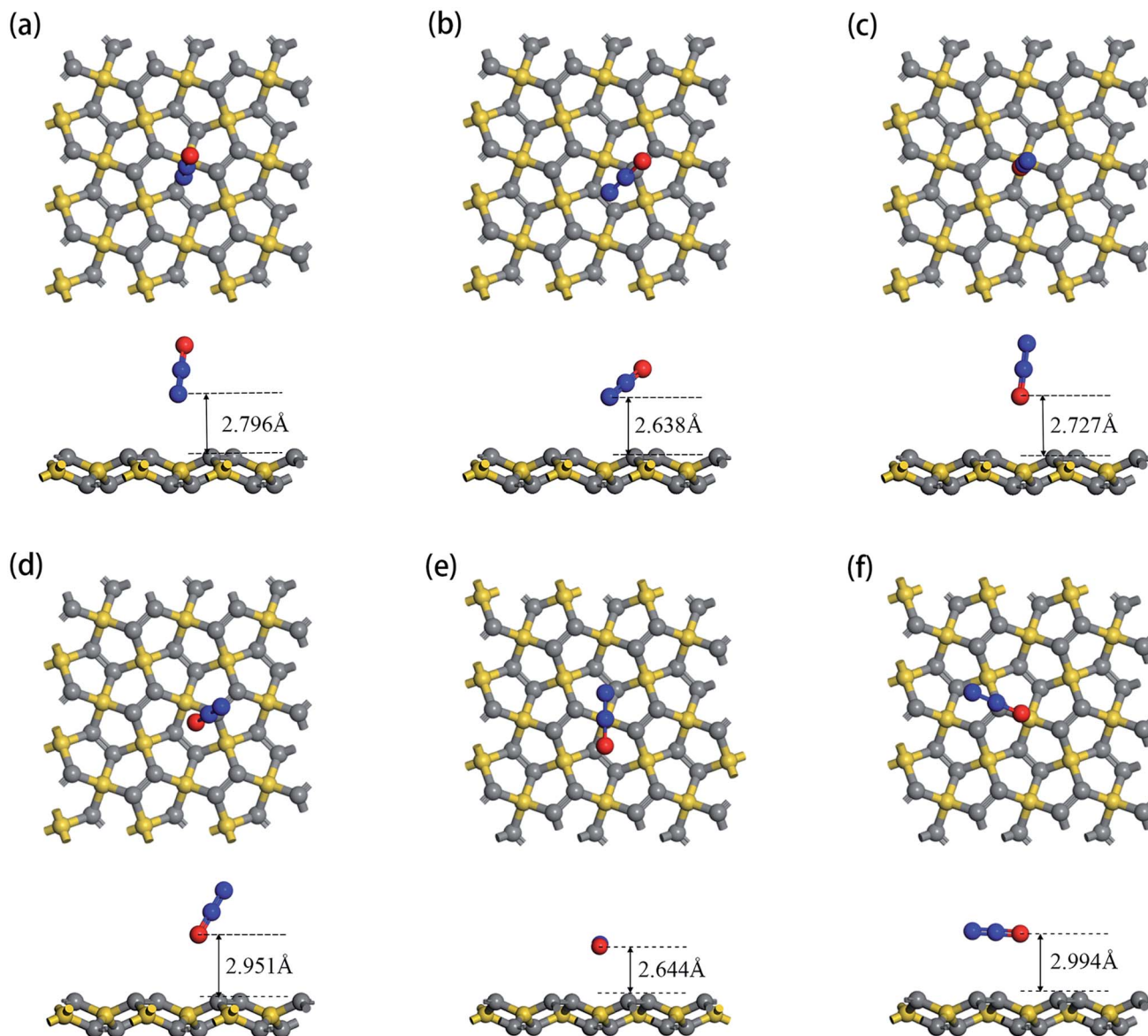


Fig. 2 Top view and side view of relaxed geometry structure of  $\text{N}_2\text{O}$  molecule adsorbed on primitive PG sheet by different forms:  $\text{N}_2\text{O}$  is vertical to PG with its O end upward at C1 site (a) and C2 site (b);  $\text{N}_2\text{O}$  is vertical to PG with its O end downward at C1 site (c) and C2 site (d);  $\text{N}_2\text{O}$  is horizontal to PG at C1 site (e) and C2 site (f).

$-0.091$  eV. Simultaneously, the  $\text{N}_2\text{O}$  molecules act as electron acceptors during the adsorption process, obtaining trace amounts of electrons from the PG sheet, which are around

Table 2 The adsorption energy  $E_{\text{ad}}$ , charge transfer  $Q$ , and band gap  $E_{\text{g}}$  of  $\text{N}_2\text{O}$  adsorbed on the PG sheet

Orientation	Adsorption site	$E_{\text{ad}}$ (eV)	$E_{\text{g}}$ (eV)	$Q$ (e)
N end	C1	$-0.114$	2.195	0.010
N end	C2	$-0.152$	2.193	0.010
O end	C1	$-0.091$	2.197	0.011
O end	C2	$-0.102$	2.198	0.009
Horizontal	C1	$-0.203$	2.197	0.015
Horizontal	C2	$-0.156$	2.189	0.018

$0.01e$ . With  $\text{N}_2\text{O}$  adsorption, the band gaps of PG slightly decreased by around  $0.01$  eV, which is almost negligible. Combined with relatively small amounts of charge transfer, weak adsorption energies and large substrate-molecule adsorption distances, we believe that  $\text{N}_2\text{O}$  molecules are physically adsorbed on the PG monolayer *via* van der Waals forces, and primitive PG is not a good choice for adsorbing and detecting the  $\text{N}_2\text{O}$  gas molecule.

### 3.2. The Ni-doped PG

Since the adsorption of  $\text{N}_2\text{O}$  gas molecules on the intrinsic PG is weak physical adsorption, the doping of transition metal Ni on PG is considered to modify the electronic properties of PG and enhance the adsorption of  $\text{N}_2\text{O}$  on PG. Two different doping



**Table 3** The binding energy  $E_b$ , band gap  $E_g$  and charge transfer  $Q$  of Ni-1-PG and Ni-2-PG

System	$E_b$ (eV)	$E_g$ (eV)	$Q$ (e)
Ni-1-PG	-6.742	1.180	-0.643
Ni-2-PG	-5.037	0.159	-0.560

sites, C1 and C2, are used for Ni atoms to decorate after the formation of C1 and C2 vacancies, and these two systems are defined as Ni-1-PG and Ni-2-PG, respectively. The binding energy, band gap and charge transfer of Ni-doped PG are listed in Table 3. The binding energies of Ni-1-PG and Ni-2-PG are -6.742 eV and -5.037 eV, respectively; the charge transfer from the Ni atom to its adjacent C atoms is 0.643e and 0.560e, which helped in the stabilization of the structures.<sup>24</sup> The calculated PDOS results are shown in Fig. 3, and strong overlapping peaks can be observed below and above the Fermi level. This reveals that the Ni atom can use its valence electrons to saturate the dangling-bond states around the vacancy site, and such strong coupling between the C-2p and Ni-3d states can maintain the Ni atom stability of the defect site. Moreover, the doping of the Ni atom significantly reduces the band gap of the structure. For Ni-1-PG, the value of the band gap decreases from 2.21 eV to 1.18 eV because new bands appear in the valence band in the band gap. While for Ni-2-PG, it decreases to 0.159 eV since new bands appear in both the valence and conduction bands of the gap. These consequences are due to the fact that donor atom Ni spreads its excess electrons to its surroundings, losing 0.643e and 0.560e at the C1 and C2 sites, respectively.

The optimized geometric configurations of N<sub>2</sub>O adsorbed on Ni-1-PG and Ni-2-PG by pointing its N or O atom to the adsorption positions are shown in Fig. 4. The values of adsorption energy, adsorption distance, band gap and charge transfer of these adsorption configurations are summarized in Table 4. For N<sub>2</sub>O adsorbed on Ni-1-PG systems, the adsorption energies are quite small, which are -0.077 eV, -0.107 eV, -0.056 eV, -0.072 eV, -0.178 eV and -0.089 eV. Furthermore, the adsorption distances are rather large, which are 2.451 Å, 2.382 Å, 2.436 Å, 2.474 Å, 2.502 Å and 3.009 Å. Moreover, after

N<sub>2</sub>O adsorption, the band gap  $E_g$  slightly increases and the N<sub>2</sub>O gas molecule only gets less than 0.02 electrons for these six configurations. We take the configuration N<sub>2</sub>O1V2 as an example to plot the differential charge density, band structure and DOS, as shown in Fig. 5a and b. The band gap slightly increased from 1.180 eV to 1.192 eV after adsorption, and there is not any hybrid coupling in the band gap from the DOS of N<sub>2</sub>O molecules and Ni-1-PG, whose corresponding orbital contributions to the adsorption systems occurred at a position far away from the Fermi level. In addition, the charge accumulation and charge depletion regions are around the gas molecule and substrate, and few overlapping areas can be observed between the electron cloud of N<sub>2</sub>O and Ni-1-PG in Fig. 5a. This means that compared with the properties of N<sub>2</sub>O on primitive PG, the adsorption between the N<sub>2</sub>O molecule and Ni-1-PG sheet is improved but is still weak physical adsorption. Therefore, Ni-1-PG is not sensitive to N<sub>2</sub>O molecules and is inadvisable for detecting or eliminating N<sub>2</sub>O molecules in general.

In contrast, Ni-2-PG exhibits excellent adsorption performance for N<sub>2</sub>O, which is affected by the adsorption orientations. When the O atom is upward, the adsorption energies are quite large and the adsorption distances are very small. N<sub>2</sub>O2V1 has better adsorption stability, with an adsorption energy of -0.944 eV and a shorter adsorption distance of 1.690 Å. This adsorption energy is larger than that of N<sub>2</sub>O adsorbed on Al-doped graphene ( $E_{ad} = -0.57$  eV),<sup>36</sup> Fe-doped MoSe<sub>2</sub> ( $E_{ad} = -0.40$  eV),<sup>37</sup> and B-doped C<sub>3</sub>N nanosheet ( $E_{ad} = -0.80$  eV).<sup>38</sup> When the O atom is downward, or N<sub>2</sub>O is horizontal, the adsorption energies are smaller and the adsorption distances are longer compared with those of N<sub>2</sub>O2V1 and N<sub>2</sub>O2V2. For example, N<sub>2</sub>O2V4 has less adsorption stability with an adsorption energy of -0.344 eV and a long adsorption distance of 2.046 Å. The differential charge density, band structure and DOS of N<sub>2</sub>O2V1 and N<sub>2</sub>O2V4 are plotted in Fig. 5c-f. For N<sub>2</sub>O2V1, N<sub>2</sub>O acts as an electron acceptor and has a large amount of charge (0.125e) from Ni-2-PG during the adsorption process. The charge interaction between N<sub>2</sub>O and substrate is quite obvious (Fig. 5c). The band gap increases after the adsorption process, but the orbital of the N<sub>2</sub>O molecules exhibits hybrid coupling with that of Ni-2-PG around the Fermi level (Fig. 5d), suggesting

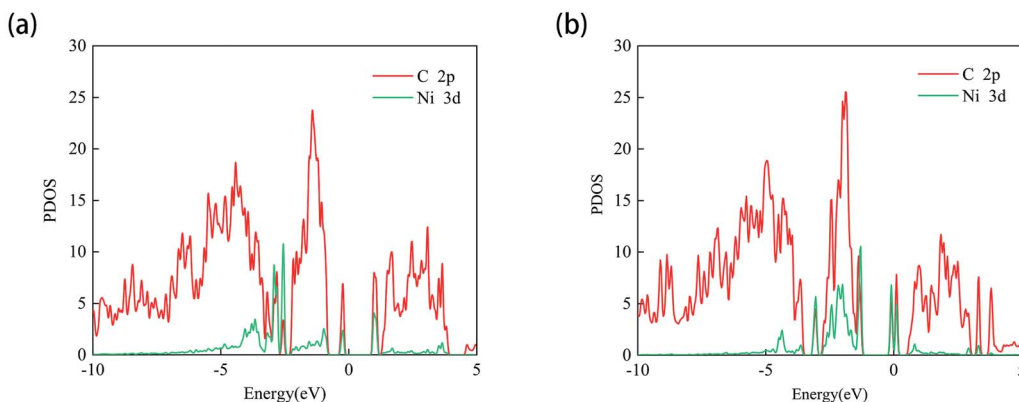


**Fig. 3** PDOS of the Ni-1-PG (a) and Ni-2-PG (b) systems. The Fermi level is set to zero.



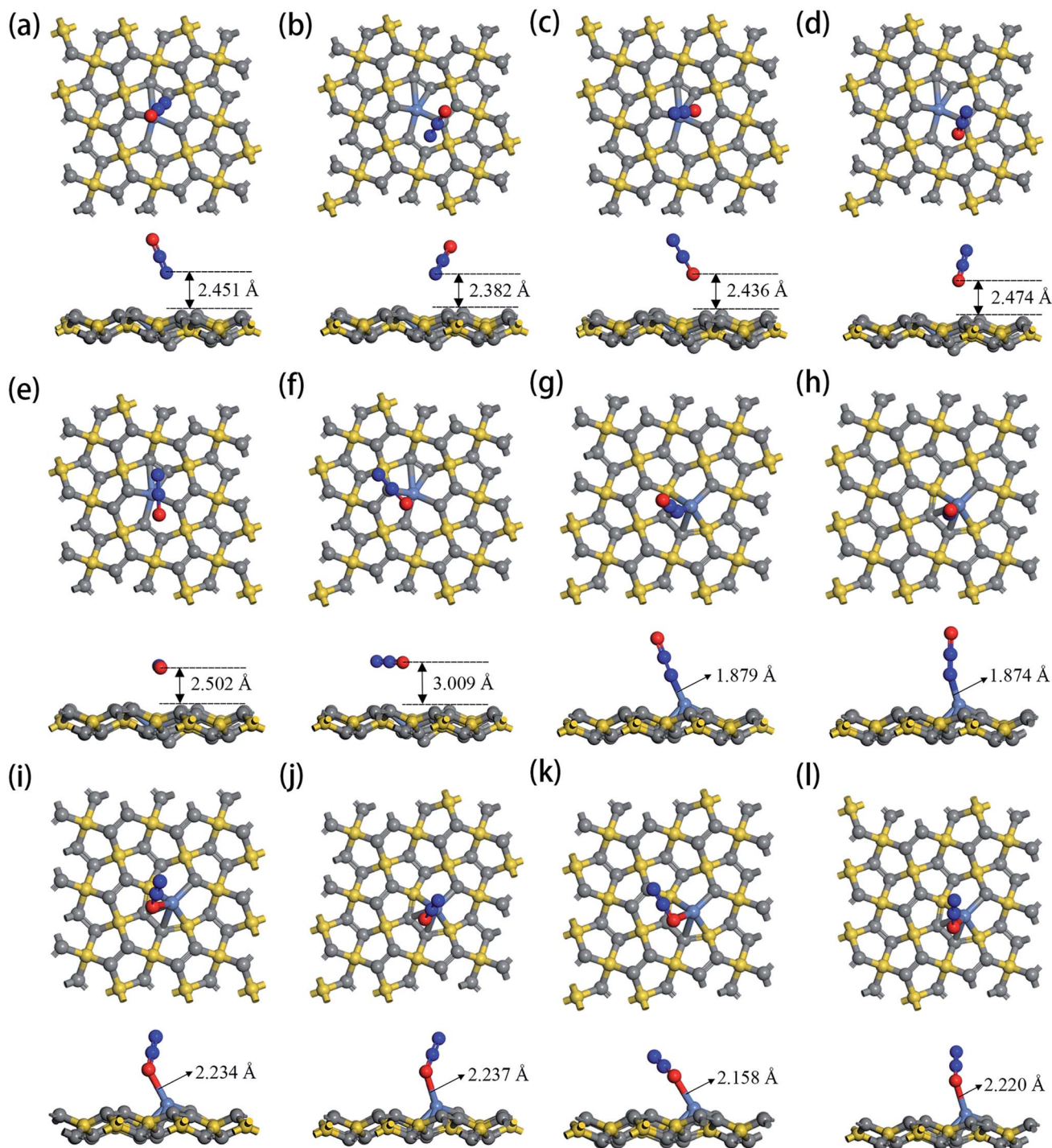


Fig. 4 Top and side views of optimized configurations of  $\text{N}_2\text{O}$  adsorbed on Ni-1-PG and Ni-2-PG: (a)  $\text{N}_2\text{O1V1}$ , (b)  $\text{N}_2\text{O1V2}$ , (c)  $\text{N}_2\text{O1V3}$ , (d)  $\text{N}_2\text{O1V4}$ , (e)  $\text{N}_2\text{O1H1}$ , (f)  $\text{N}_2\text{O1H2}$ , (g)  $\text{N}_2\text{O2V1}$ , (h)  $\text{N}_2\text{O2V2}$ , (i)  $\text{N}_2\text{O2V3}$ , (j)  $\text{N}_2\text{O2V4}$ , (k)  $\text{N}_2\text{O2H1}$ , and (l)  $\text{N}_2\text{O2H2}$ .

that the interaction between the  $\text{N}_2\text{O}$  gas molecule and Ni-2-PG is strong and the  $\text{N}_2\text{O}$  molecule is chemically adsorbed on Ni-2-PG. For  $\text{N}_2\text{O2V4}$ , the band gap was further increased, and the corresponding orbital contribution of the adsorption system occurred at a position far away from the Fermi level, so the  $\text{N}_2\text{O}$  molecule could only obtain a small amount of charge from Ni-2-PG. However, Fig. 5e shows an overlapped charge interaction

region between the  $\text{N}_2\text{O}$  molecule and substrate, which indicates that the configuration  $\text{N}_2\text{O2V4}$  is still chemical adsorption. In general, the adsorption strength of  $\text{N}_2\text{O}$  is determined by the adsorption orientation: when the O atom is downward, the adsorption strength is relatively weaker, which indicates that the  $\text{N}_2\text{O}$  molecule is likely to be desorbed from Ni-2-PG within these adsorption configurations; when the O atom is

**Table 4** The calculated adsorption energy  $E_{ad}$ , adsorption distance  $d$ , band gap  $E_g$  and charge transfer  $Q$  of different orientations of  $N_2O$  adsorbed on Ni-1-PG and Ni-2-PG

System	Orientation	$E_{ad}$ (eV)	$d$ (Å)	$E_g$ (eV)	$Q$ (e)
$N_2O$ on Ni-1-PG	Vertical to C1 and O is upward( $N_2O1V1$ )	-0.077	2.451	1.201	0.012
	Vertical to C2 and O is upward ( $N_2O1V2$ )	-0.107	2.382	1.192	0.011
	Vertical to C1 and O is downward( $N_2O1V3$ )	-0.056	2.436	1.192	0.013
	Vertical to C2 and O is downward( $N_2O1V4$ )	-0.072	2.474	1.182	0.011
	Horizontal to C1( $N_2O1H1$ )	-0.178	2.502	1.211	0.019
	Horizontal to C2( $N_2O1H2$ )	-0.089	3.009	1.171	0.018
$N_2O$ on Ni-2-PG	Vertical to C1 and O is upward( $N_2O2V1$ )	-0.944	1.690	0.421	0.125
	Vertical to C2 and O is upward ( $N_2O2V2$ )	-0.935	1.749	0.429	0.128
	Vertical to C1 and O is downward( $N_2O2V3$ )	-0.346	1.956	0.430	0.007
	Vertical to C2 and O is downward( $N_2O2V4$ )	-0.344	2.046	0.436	0.006
	Horizontal to C1( $N_2O2H1$ )	-0.453	1.798	0.305	0.002
	Horizontal to C2( $N_2O2H2$ )	-0.358	2.035	0.452	0.006

upward, the adsorption behavior is much stronger, and  $N_2O$  molecule can be stably adsorbed on Ni-2-PG substrate.

Furthermore, the partial density of states (PDOS) of  $N_2O2V1$  and  $N_2O2V4$  are plotted to further investigate the adsorption effect of  $N_2O$  on Ni-2-PG, and the results are shown in Fig. 6. For configuration  $N_2O2V1$ , obvious orbital mixing exists between the  $N_2O$  and substrate at the position very close to the Fermi level: the p orbital of  $N_1$  and O atoms in  $N_2O$  overlap with the p and d orbitals of Ni on the surface of Ni-2-PG, at about -0.225 eV; the s and p orbitals of  $N_1$ , p orbital of  $N_2$  and O atom overlap with the s, p and d orbitals of Ni, at about -1.241 eV. Furthermore, the p orbitals of  $N_2$  and O atoms in  $N_2O$  have large overlapping peaks with the s, p and d orbitals of the Ni atom at about -4.437 eV, a little far away from the Fermi level. These results indicate that  $N_2O2V1$  has stable and strong chemical adsorption performance. While for configuration  $N_2O2V4$ , the relatively overlapping area of the formant is far away from the Fermi level: the p orbitals of  $N_1$ ,  $N_2$  and O atoms in  $N_2O$  overlap the s, p and d orbitals of Ni atom at about -4.923 eV and -5.178 eV. This means that a chemical bond is formed between the  $N_2O$  gas molecule and the Ni-2-PG substrate, but the bond is weaker than that of  $N_2O2V1$  due to its relatively far and tiny overlapping area. The analysis discussed above demonstrates that Ni-2-PG has a greater adsorption performance, and the  $N_2O$  molecule can be chemisorbed on it regardless of the adsorption orientation.

### 3.3. Applied electric field

Since the external electric field can influence the adsorption property by adjusting the internal charge state,<sup>39-41</sup> we applied an external perpendicular electric field to the adsorption configuration, and  $N_2O2V2$  was chosen as a candidate. As shown in Fig. 7a, the direction from the substrate toward the gas molecule (upward) is positive, whereas the opposite direction (downward) is negative. Fig. 7b displays the change in the adsorption energy with respect to the electric field from  $-0.5 \text{ V \AA}^{-1}$  to  $+0.5 \text{ V \AA}^{-1}$ . It can be seen that the adsorption energy of

$N_2O$  shows a significant increase with the increase in the electric field strength when either a positive or negative electric field is applied, except for the positive electric field value of  $+0.1 \text{ V \AA}^{-1}$ , whose adsorption energy decreases to the minimum. Under the electric field value of  $+0.5 \text{ V \AA}^{-1}$ , the adsorption energy increases to  $-1.195 \text{ eV}$ , which is 28% higher than that with no extra electric field. As mentioned above, the property of adsorption energy under the electric field varies because of the adjustment of the atomic charge state between the adsorbed gas molecule and the substrate, which may be caused by charge transfer, adsorption structure, and adsorption distance. Fig. 7c-e show the change curves of the charge transfer, the bond lengths of the  $N_2O$  molecule ( $l_{N_1-O}$  and  $l_{N_1-N_2}$ ) and the formed chemical bond ( $l_{N_2-Ni}$ ) as a function of the electric field. The positive electric field is capable of promoting the charge transfer process from the substrate to the adsorbed molecule, whereas the negative electric field hinders the charge transfer induced by  $N_2O$  adsorption. It was observed that the charge transfer from the Ni-2-PG substrate to the  $N_2O$  gas molecule increased linearly when the electric field changed from  $-0.1 \text{ V \AA}^{-1}$  to  $+0.5 \text{ V \AA}^{-1}$ . When the electric field reached  $+0.5 \text{ V \AA}^{-1}$ ,  $N_2O$  achieves additional 0.028 electrons arising from the Ni-2-PG substrate. This alteration of charge transfer may be relevant to the dipole moment emerging between the adsorbed gas molecule and substrate,<sup>42</sup> which shows that the same directions of electric field and dipole moment enhance charge transfer while opposite directions weaken it. Furthermore, the dipole moment and charge transfer between the substrate and  $N_2O$  further enhance the charge redistribution on the surface of Ni-2-PG, which is why the bond length  $l_{N_2-Ni}$  decreases with an increase in the electric field. This means that the adsorption distance decreases when the electric field is positive and increases when the electric field is negative. Moreover, the variation curves of the bond length  $l_{N_1-O}$  and  $l_{N_1-N_2}$  of the  $N_2O$  gas molecule are plotted in Fig. 7d. With an increase in the applied electric field from negative to positive, the bond length between  $N_1$  and O atoms significantly increases, whereas the



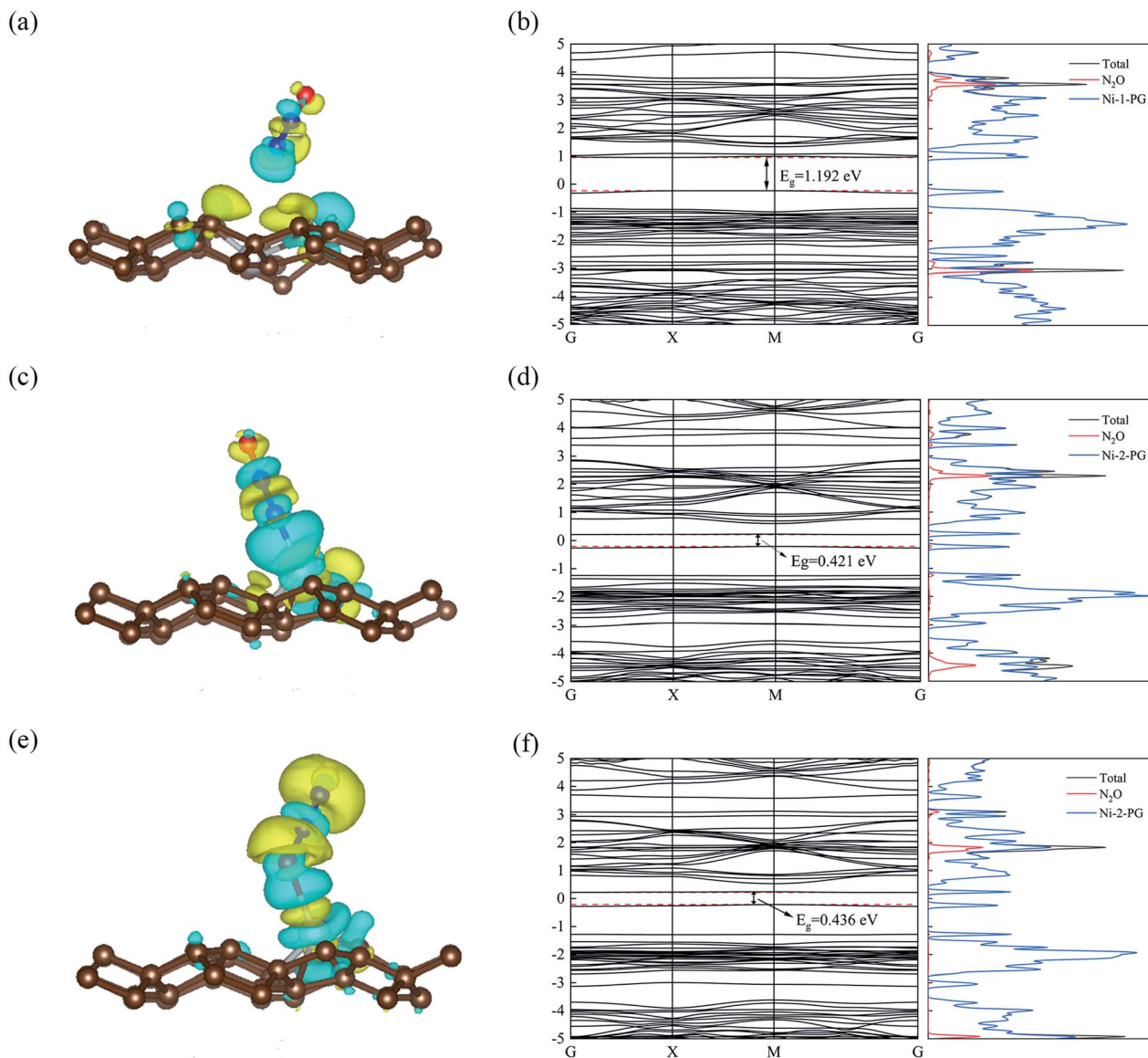


Fig. 5 The differential charge densities of the relaxed configuration: (a) N<sub>2</sub>O1V2 (c) N<sub>2</sub>O2V1 and (e) N<sub>2</sub>O2V4; the isovalues are 0.0002 a.u., 0.0009 a.u. and 0.0004 a.u., respectively; the blue and yellow represent the gain and loss of electrons, respectively. (b), (d) and (f) denote the band structure and DOS of N<sub>2</sub>O1V2, N<sub>2</sub>O2V1 and N<sub>2</sub>O2V4. The Fermi level is set to zero.

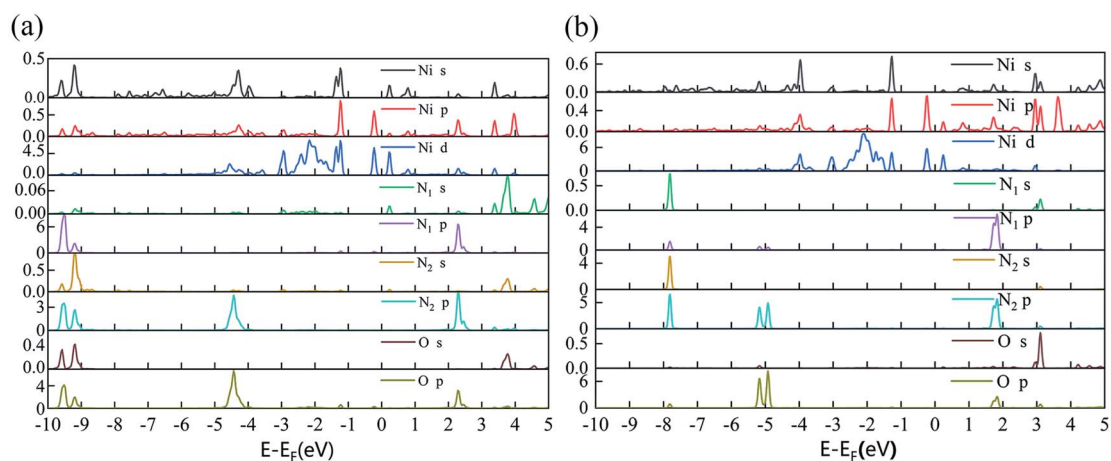


Fig. 6 The partial density of states of configuration: (a) N<sub>2</sub>O2V1 and (b) N<sub>2</sub>O2V4.

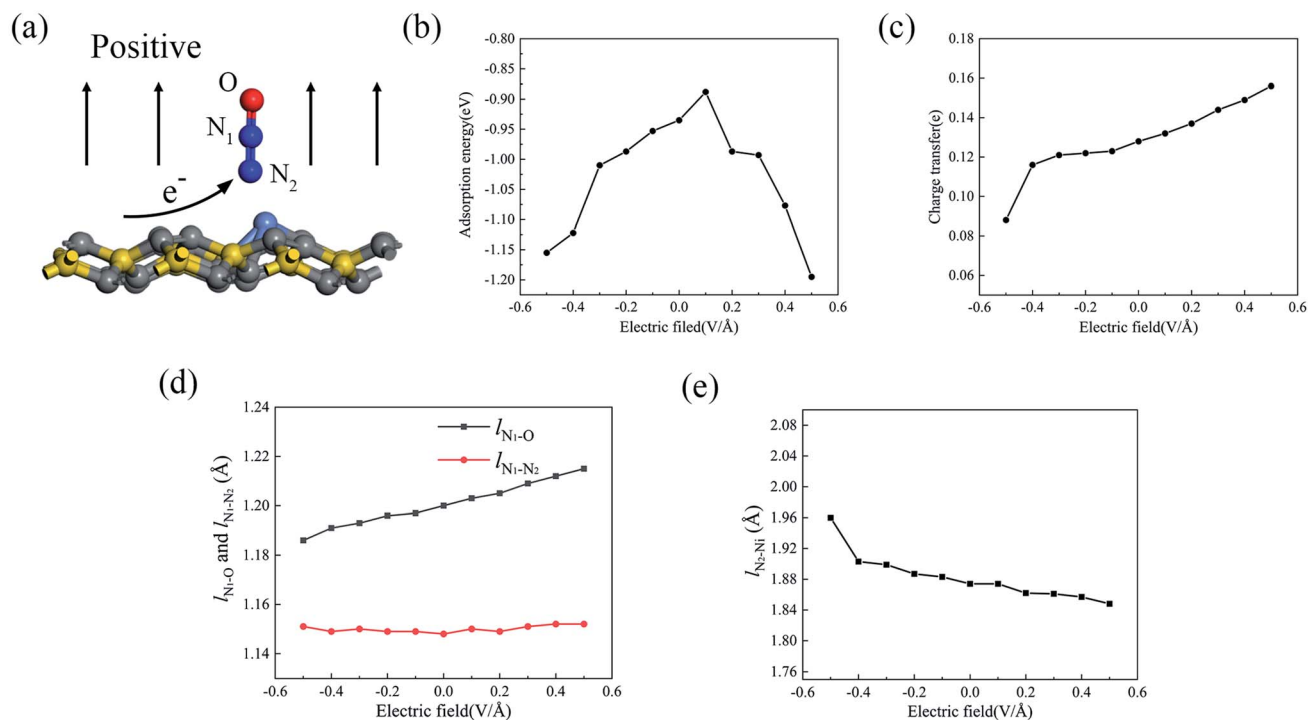


Fig. 7 (a) The diagram of the N<sub>2</sub>O<sub>2</sub>V<sub>2</sub> under a positive external perpendicular electric field. The variation curves of (b) adsorption energy, (c) charge transfer, (d)  $l_{\text{Ni-O}}$  and  $l_{\text{Ni-N}_2}$ , and (e)  $l_{\text{N}_2\text{-Ni}}$  of N<sub>2</sub>O<sub>2</sub>V<sub>2</sub> as a function of the electric fields.

distance between N<sub>1</sub> and N<sub>2</sub> atoms remains almost constant at about 1.50 Å. Because the p orbital of the O atom plays an important role in the formation of chemical bonds in the adsorption process, when a negative electric field is applied, the bond length  $l_{\text{Ni-O}}$  decreases, causing a large adsorption energy and more stable adsorption.

In most cases, an external perpendicular electric field can remarkably enhance the adsorption energy and adsorption performance of the N<sub>2</sub>O molecule, which is not affected by the direction of the electric field when the value is greater than 0.1 V Å<sup>-1</sup>. Based on this result, we suggest that applying an electric field is an essential and favorable method for improving the sensitivity of the Ni-2-PG sensors to N<sub>2</sub>O gas molecules. This result is in good agreement with previous studies, which inferred that an external perpendicular electric field would enhance the adsorption behaviors both theoretically<sup>43,44</sup> and experimentally.<sup>45</sup>

## 4. Conclusion

In this study, the adsorption behaviors of N<sub>2</sub>O on PG and Ni-doped PG were theoretically investigated using first-principles calculations. By comparing and analyzing the results of adsorption energy, charge transfer, band gap, DOS and PDOS, we observed that the N<sub>2</sub>O molecule was physically adsorbed *via* van der Waals forces on the intrinsic PG and Ni-1-PG, whereas N<sub>2</sub>O was chemically adsorbed on Ni-2-PG, forming chemical bonds between the gas molecule and substrate. Therefore, the N<sub>2</sub>O molecule can be stably adsorbed on the Ni-doped PG only when the Ni atom is doped at the sp<sup>2</sup> hybridized carbon site

(C2). Additionally, the adsorption behaviors were affected by the adsorption orientations, in which the N<sub>2</sub>O molecule with its N atom close to the substrate exhibited better adsorption stability. Moreover, the application of a perpendicular electric field can improve the sensitivity of Ni-2-PG to N<sub>2</sub>O by enhancing the adsorption ability and adjusting the charge distribution between the gas molecule and substrate. Therefore, the adsorption application of PG could be broadened to N<sub>2</sub>O, and Ni-2-PG could be a promising candidate for the adsorption or detection of N<sub>2</sub>O gas molecules.

## Conflicts of interest

There are no conflicts to declare.

## Acknowledgements

The first-principles calculations in this work are based on the VASP package, which is provided by Prof. Gang Zhou in Hubei University of Technology. This work is also supported by the National Natural Science Foundation of China under Grants No. 11404119, by the Doctoral Scientific Research Foundation of Hubei University of Technology (Grant No. BSQD2020106).

## References

- 1 S. Zhang, J. Zhou, Q. Wang, X. Chen, Y. Kawazoe and P. Jena, *Proc. Natl. Acad. Sci. U. S. A.*, 2015, **112**, 2372–2377.
- 2 H. Sun, S. Mukherjee and C. V. Singh, *Phys. Chem. Chem. Phys.*, 2016, **18**, 26736–26742.



- 3 F. Q. Wang, J. Yu, Q. Wang, Y. Kawazoe and P. Jena, *Carbon*, 2016, **105**, 424–429.
- 4 Z. Wang, F. Dong, B. Shen, R. Zhang, Y. Zheng, L. Chen, S. Wang, C. Wang, K. Ho and Y.-J. Fan, *Carbon*, 2016, **101**, 77–85.
- 5 J. Deb, N. Seriani and U. Sarkar, *Phys. E*, 2021, **127**, 114507.
- 6 B. Xiao, Y.-c. Li, X.-f. Yu and J.-b. Cheng, *ACS Appl. Mater. Interfaces*, 2016, **8**, 35342–35352.
- 7 R. Krishnan, W.-S. Su and H.-T. Chen, *Carbon*, 2017, **114**, 465–472.
- 8 M.-Q. Cheng, Q. Chen, K. Yang, W.-Q. Huang, W.-Y. Hu and G.-F. Huang, *Nanoscale Res. Lett.*, 2019, **14**, 1–8.
- 9 T. Y. Mi, D. M. Triet and N. T. Tien, *Physics Open*, 2020, **2**, 100014.
- 10 C. Feng, X.-H. Luan, P. Zhang, J. Xiao, D.-G. Yang and H.-B. Qin, A first-principle study of the adsorption behavior of NO gas molecules on pristine and Al-doped penta-graphene, *2017 18th International Conference on Electronic Packaging Technology (ICEPT)*, 2017, pp. 1138–1142, DOI: [10.1109/ICEPT.2017.8046642](https://doi.org/10.1109/ICEPT.2017.8046642).
- 11 Y. Ni, J. Li, W. Tao, H. Ding and R.-X. Li, *Phys. Chem. Chem. Phys.*, 2021, **23**, 2753–2761.
- 12 H. Li, Q. Zhang, C. C. R. Yap, B. K. Tay, T. H. T. Edwin, A. Olivier and D. Baillargeat, *Adv. Funct. Mater.*, 2012, **22**, 1385–1390.
- 13 E. Bengu and L. Marks, *Phys. Rev. Lett.*, 2001, **86**, 2385.
- 14 S.-C. Zhu, C.-T. Yip, S.-J. Peng, K.-M. Wu, K.-L. Yao, C.-L. Mak and C.-H. Lam, *Phys. Chem. Chem. Phys.*, 2018, **20**, 7635–7642.
- 15 N. Liu, J. Liu, S. Wang and K. Yao, *Phys. Lett. A*, 2020, **384**, 126127.
- 16 Y. Feng, X. Wu, J. Han and G. Gao, *J. Mater. Chem. C*, 2018, **6**, 4087–4094.
- 17 Y. Ni, H. Hua, J. Li and N. Hu, *Nanoscale*, 2022, **14**, 3818–3825.
- 18 H. Qin, C. Feng, X. Luan and D. Yang, *Nanoscale Res. Lett.*, 2018, **13**, 1–7.
- 19 J. I. G. Enriquez and C. V. Al Rey, *Int. J. Hydrogen Energy*, 2016, **41**, 12157–12166.
- 20 C.-P. Zhang, B. Li and Z.-G. Shao, *Appl. Surf. Sci.*, 2019, **469**, 641–646.
- 21 X. Zhang, X. Wang, X. Zhao, Y. Xu, H. Gao and F. Zhang, *Chem. Eng. J.*, 2014, **252**, 288–297.
- 22 J. M. Otte, N. Blackwell, R. Ruser, A. Kappler, S. Kleindienst and C. Schmidt, *Sci. Rep.*, 2019, **9**, 1–12.
- 23 M. Cain, J. Lynch, M. R. Allen, J. S. Fuglestedt, D. J. Frame and A. H. Macey, *npj Clim. Atmos. Sci.*, 2019, **2**, 1–7.
- 24 M. D. Esrafil and N. Saeidi, *New J. Chem.*, 2017, **41**, 13149–13155.
- 25 H. Wei, Y. Gui, J. Kang, W. Wang and C. Tang, *Nanomaterials*, 2018, **8**, 646.
- 26 H. Cui, X. Zhang, Y. Li, D. Chen and Y. Zhang, *Appl. Surf. Sci.*, 2019, **494**, 859–866.
- 27 H. Wang, Q. Wang, Y. Cheng, K. Li, Y. Yao, Q. Zhang, C. Dong, P. Wang, U. Schwingenschlögl and W. Yang, *Nano Lett.*, 2012, **12**, 141–144.
- 28 F. Banhart, J. Kotakoski and A. V. Krasheninnikov, *ACS Nano*, 2011, **5**, 26–41.
- 29 G. Kresse and J. Furthmüller, *Comput. Mater. Sci.*, 1996, **6**, 15–50.
- 30 G. Kresse and J. Furthmüller, *Phys. Rev. B*, 1996, **54**, 11169.
- 31 F. Neese, F. Wennmohs, A. Hansen and U. Becker, *Chem. Phys.*, 2009, **356**, 98–109.
- 32 J. P. Perdew, K. Burke and M. Ernzerhof, *Phys. Rev. Lett.*, 1996, **77**, 3865.
- 33 K. Yang, J. Zheng, Y. Zhao and D. G. Truhlar, *J. Chem. Phys.*, 2010, **132**, 164117.
- 34 S. Grimme, *J. Comput. Chem.*, 2006, **27**, 1787–1799.
- 35 B. Rajbanshi, S. Sarkar, B. Mandal and P. Sarkar, *Carbon*, 2016, **100**, 118–125.
- 36 Y.-a. Lv, G.-l. Zhuang, J.-g. Wang, Y.-b. Jia and Q. Xie, *Phys. Chem. Chem. Phys.*, 2011, **13**, 12472–12477.
- 37 N. Mishra, B. P. Pandey, B. Kumar and S. Kumar, *Superlattices Microstruct.*, 2021, **160**, 107083.
- 38 M. D. Esrafil and S. Heidari, *Chem. Phys. Lett.*, 2019, **725**, 52–58.
- 39 X. F. Yu, Y. C. Li, J. B. Cheng, Z. B. Liu, Q. Z. Li, W. Z. Li, X. Yang and B. Xiao, *ACS Appl. Mater. Interfaces*, 2015, **7**, 13707–13713.
- 40 S. Ma, D. Yuan, Z. Jiao, T. Wang and X. Dai, *J. Phys. Chem. C*, 2017, **121**, 24077–24084.
- 41 X.-Y. Liang, N. Ding, S.-P. Ng and C.-M. L. Wu, *Appl. Surf. Sci.*, 2017, **411**, 11–17.
- 42 S. Tang and Z. Cao, *J. Chem. Phys.*, 2011, **134**, 044710.
- 43 N. Sathishkumar, S.-Y. Wu and H.-T. Chen, *Chem. Eng. J.*, 2020, **391**, 123577.
- 44 N. Sathishkumar, S.-Y. Wu and H.-T. Chen, *Chem. Eng. J.*, 2021, **407**, 127194.
- 45 T. E. Benavidez, D. Torrente, M. Marucho and C. D. Garcia, *Langmuir*, 2015, **31**, 2455–2462.

